Pharm Res (2013) 30:1252–1262
DOI 10.1007/s11095-012-0964-5

RESEARCH PAPER

Engineered Andrographolide Nanoparticles Mitigate Paracetamol Hepatotoxicity in Mice

Partha Roy • Suvadra Das • Runa Ghosh Auddy • Achintya Saha • Arup Mukherjee

Received: 7 August 2012 / Accepted: 13 December 2012 / Published online: 15 January 2013

ABSTRACT

Purpose Paracetamol (acetaminophen, APAP) overdose is often fatal due to progressive and irreversible hepatic necrosis. The aim of this work was to design Andrographolide (AG) loaded nanoparticles to prevent similar hepatic necrosis.

Methods Functionalized AG-loaded PLGA nanoparticles carrying different densities of heparin were prepared following a facile emulsion solvent evaporation technique. Nanoparticle morphology, loading and release kinetics were studied. Hepatic localization of the nanoparticles was investigated in both normal and APAP damaged conditions using FITC fluorescent probe. Different serum parameters and liver histopathology were further examined as indicators of hepatic condition before and after treatment.

Result A collection of heparin functionalized AG-loaded PLGA nanoparticles were designed. Low amount of heparin on the particle surface could rapidly localize the nanoparticles up to the liver. The new functionalized AG nanoparticles affect efficient hepatoprotection in experimental mouse APAP overdose conditions. AG nanoparticle hepatoprotection was due to the rapid regeneration of antioxidant capacity and hepatic GSH store.

Conclusions Engineered nanoparticles loaded with AG provided a fast protection in APAP induced acute liver failure.

KEY WORDS andrographolide · GSH · heparin · liver · paracetamol

P. Roy • S. Das • R. G. Auddy • A. Saha • A. Mukherjee (✉)
Division of Pharmaceutical and Fine Chemicals Technology
Department of Chemical Technology
University of Calcutta, 92, APC Road
Kolkata 700009, India
e-mail: arupm1234@gmail.com

A. Mukherjee
e-mail: hdct1@yahoo.co.in

ABBREVIATIONS

AG	andrographolide
AGnp	andrographolide nanoparticle
APAP	N-acetyl-p-aminophenol
BCS	biopharmaceutical classification system
CT	computed tomography
CTCF	corrected total cell fluorescence
DILD	drug induced liver damage
FITC	fluorescein isothiocyanate
Fnp	fluorescent nanoparticle
Hep	heparin
Hep-Fnp	heparinized fluorescent nanoparticle
Hep-AGnp	heparin functionalized andrographolide nanoparticle
KCE	known chemical entity
MDA	malondialdehyde
Mrp	multi-drug resistance protein
NAC	N-acetyl cysteine
NAPQI	N-acetyl-para benzoquinoneimine
PEO	polyethylene oxide
PLGA	poly (D-L-lactide-co-glycolic acid)
PPO	polypropylene oxide
ROS	reactive oxygen species

INTRODUCTION

APAP is the most widely used over the counter analgesic antipyretic drug. The drug is apparently safe in therapeutic dosage. However in higher dose or in case of liver injury, the drug is associated with a significant morbidity and mortality. Overdose is in fact, the leading cause for drug induced liver damage (DILD) in the United States and Great Britain (1). APAP is normally detoxified in human as soluble glucuronide and sulfonate by the phase II metabolizing enzymes. A part, but gets converted in cytochrome P450 system to a

highly reactive species N-acetyl-para benzoquinone imine (NAPQI) (2). NAPQI once formed, readily reacts with hepatic glutathione (GSH) and the resultant GSH-adduct is excreted in bile with Mrp2 protein (3). In case of depleted hepatic GSH level as in APAP overdose, in alcoholics, or in case of antiretroviral therapy, cancer chemotherapy or in conditions of DILD, NAPQI irreversibly binds with a number of intracellular target proteins inducing mitochondrial oxidative stress (4). The metabolic activation of APAP further leads to membrane disintegration, depletion of ATP, DNA fragmentation and culminate in necrosis of liver cells (5). The US FDA advisory committee has recently warranted new restrictions to protect against the toxic effects and suicidal consumption of this drug. N-acetyl cysteine (NAC) administered under hospital care for a prolonged period is currently recommended as the only remedy. NAC helps to restore the depleted GSH store but, is associated with several side effects and is effective only within 12 h of APAP ingestion (6). Currently, there is a great demand for an out of shelf therapeutic in conditions like APAP hepatotoxicity.

AG is a diterpenoid lactone isolated from the leaves of *Andrographis paniculata*. AG is a known chemical entity (KCE) and interacts with a diverse range of biomolecular targets (7). Hepatoprotective activity of AG is pronounced due to activation of antioxidant enzymes, membrane stabilization and restoration of hepatic GSH levels (8). The KCE is also a strong inhibitor of angiogenesis pathways (9). AG however is BCS case IV type, having low water solubility, low permeability and a low biological $t_{1/2}$ of 2 h (10). This has marred all further therapeutic applications of AG.

Nanoparticle engineering in an US FDA approved biopolymer PLGA was conceived to explore the therapeutic potentials of AG. Heparin is a linear natural polysaccharide composed of sulfonated glucuronic and glucosamine derivatives and is used as a systemic anticoagulant agent. Heparin showed large accumulation in Kupffer cells and in endothelial like cell lining in the liver sinusoids (11). Gold nanoparticles functionalized with heparin were earlier used for guided CT (Computed tomography) imaging in hepatocellular locations (12). Heparin was also investigated as a biocompatible antifouling material for coating in medical devices and drug delivery for rapid uptake to the tissue target (13). PLGA nanoparticles functionalized with heparin in a one pot synthesis were experimented. We postulated that the new AG nanoparticles may rapidly traverse up to the liver for an effective hepatoprotection. AG biochemical pharmacology further augments hepatocellular regeneration and that would alleviate progression of hepatic necrosis. Engineered AG nanoparticles can be useful as out of shelf therapeutic in treatment of liver injury as in case of APAP poisoning.

MATERIALS AND METHODS

Materials

All solvents and water used were of HPLC grade (E. Merck, India). PLGA (50:50, MW 40,000–75,000), Dialysis tubing (MW cut off 12,400), FITC, Pluronic F-127 (MW 12,600), Heparin Sodium (MW 17,000–19,000), Toluidine-blue reagent were all purchased from Sigma-Aldrich (St. Louis, MO, USA). AG was purchased from Natural Remedies (Bangalore, India) and APAP was received as a gift from Dey's Medical Stores Kolkata India. Diagnostic kits for biochemical studies were from Merck Specialties Private Ltd (Mumbai, India). Windows Excel (v 2003; Redmond, WA), Image J (v 1.45; Maryland, USA) and Sigmaplot (v 6.0; Zendal Scientific, USA) softwares were used for most data and image analysis purposes.

Preparation of AG Nanoparticles

Nanoparticles were prepared following a facile emulsion solvent evaporation technique. Briefly, 50 mg PLGA and 2.5 mg of AG were dissolved together in 3 ml of chloroform and the organic phase was emulsified in 12 ml of aqueous solution containing different concentrations of heparin and 1%*w*/*v* pluronic F-127. Emulsification was achieved in 2 min sonication (Vibra cell VCX 750, Sonics, USA) at 75 KW, 20 KHZ followed by 20 min homogenization (TH 02, Omni International, USA) at 20,000 rpm under external cooling in ice water. The solvent evaporation was continued for 12 h over a magnetic stirrer at room temperature. AG nanoparticles formed were seceded by ultracentrifugation (Hitachi Koki, Japan) at 30,000 rpm for 25 min at 4°C. Final particles were re-dissolved in water, similarly centrifuged and preserved in desiccators at 4°C. Heparin concentration of 1 mg/ml and 2 mg/ml were used for Hep-AGnp I and Hep-AGnp II type preparations. AG nanoparticles without heparin (AGnp), were also prepared following the same procedure omitting only heparin. Fluorescently labeled nanoparticles of Fnp, Hep-Fnp I and Hep-Fnp II types were prepared similarly for a tissue localization study replacing AG with FITC.

Characterization of Nanoparticles

The particle size and polydispersity index (PDI) of all nanoparticle types were measured in a Zetasizer (Nano ZS, Malvern Instruments, UK) against 4mw He-Ne laser beam using a back scattering angle of 173°. Zeta potentials were measured on the basis of electrophoretic mobility under an applied electric field in disposable cuvettes. Particle morphology was analyzed in atomic force microscopy (Nanoscope 3A, Veeco, USA) and micrographs were obtained in tapping mode using RTESP tip

with 267–328 KHz resonance frequency at a scan speed of 1.2 Hz.

FT-IR Studies

FT-IR (670 plus, Jasco, Japan) was used extensively as a tool to understand each of the component interactions before and after nanoparticulation. AG, PLGA, Pluronic F-127 and Heparin were pelletized separately in IR grade KBr (Pike technologies, USA) and were scanned in transmittance mode over the mid IR range of 4000 to 400 cm^{-1}. Prepared nanoparticles were also pelletized separately in KBr and scanned similarly. All data were stacked in Biorad KnowItAll software (Bio-rad, USA) for analysis.

AG Entrapment

Estimation of AG was carried out in a reverse phase HPLC (Dual Pump 515,Waters, USA) running with mobile phase, acetonitrile: 0.1%*v/v* phosphoric acid in water (40:60*v/v*); at a flow rate of 1 ml/min. AG retention time recorded was 4.5 min. A peak area (y) *versus* concentration (x) graph for AG was first prepared and used to detect AG concentration throughout. Mass of AG before and after nanoparticulation in the supernatant was determined in HPLC experiments (14) in each case for calculation of entrapment efficiencies.

AG Release Studies and Release Kinetics Modeling

Individual nanoparticle types were dispersed separately in 1 ml of phosphate buffer (100 mM, pH 7.4) and washed into dialysis bags with molecular weight cut off 12,400 (Sigma, USA). The dialysis bags were placed in individual glass vials containing 10 ml of phosphate buffer maintained at 37°C over a magnetic stirrer. The release medium in vials was replaced with fresh buffer medium at predetermined time intervals and the AG released in medium per timed sample was estimated in HPLC. The release data was analyzed in Korsemeyer-Peppas model and the n and K values were derived using Sigmaplot 6.0 software.

Storage Stability Studies

Each nanoparticle types were sealed under nitrogen in amber colored glass vials in triplicate and were stored in the refrigerator (4±0.5°C) for 3 months. Aliquots were withdrawn at the end of the 1st, 2nd and 3rd month, dispersed in phosphate buffer (100 mM, pH 7.4) and particle size, polydispersity and zeta potentials were analyzed. The phosphate buffer layer was further separated by centrifugation and analyzed in HPLC.

Heparin Estimation

Heparin incorporation in nanoparticles was measured following toluidine blue colorimetric assay (15). A standard graph was first prepared from varying amount of heparin reacting with toluidine blue and recording the resultant absorbance shift at 562 nm (model 2550, Shimadzu, Japan). Free heparin content in the initial preparation solutions and in the accumulated supernatant after centrifugation and harvesting of nanoparticles were determined from the standard curve. The difference in absorbance was used for estimation of heparin entrapped.

Hepatoprotection Studies *In vivo*

Four weeks old, healthy, male Swiss albino mice (22–25 g) were used for this study. All animal experiments were conducted as per the approval of the Institutional Animal Ethics Committee, Govt. of India (Registration Number 506/05/b/CPCSEA). Laboratory animals were housed in plastic cages bedded with rice husk and were allowed to adapt for 5 days in laboratory conditions of 25±2°C and 12/12 light/dark cycles. They were given free access to standard pellet diet (Hindustan Uniliver, India) and water *ad libitum* till the day of the experiment. On the day of the experiment only water was allowed. The experiment involved six groups of eight animals each in the following treatment schedule.

- Group 1 served as control and was treated with normal saline (10 ml/kg).
- Group 2 received APAP dissolved in water.
- Group 3 received APAP and AG dissolved in DMSO (5%v/v) and dispersed in saline.
- Group 4 received APAP and AGnp dispersed in saline.
- Group 5 received APAP and Hep-AGnp I dispersed in saline.
- Group 6 received APAP and Hep-AGnp II dispersed in saline.

Liver damage was induced in mice by a single i.p. injection of 300 mg/kg APAP (16). One hour after APAP injection, group 3 animals received one i.p. injection of AG 50 mg/kg. Group 4, 5 and 6 animals were treated similarly with nanoparticles in equivalent of 50 mg/kg AG payload. Behavioral parameters were recorded after six hours of preventive therapy and animals in group 3 to 6 received a second similar injection as per schedule. Serum marker enzymes were analyzed after 12 h of APAP injection. Blood was collected by cardiac puncture under ether anesthesia for analysis of serum marker enzymes. The analysis kits and procedures used were as provided by Ecoline, Merck Specialities Pvt. Ltd. Animals were sacrificed by cervical dislocation immediately after collection of blood and the liver tissue in each case was dissected out. Liver tissues from two

animals in each group were preserved separately in 10% neutral formalin solution for microtomy. These were later dehydrated and embedded in paraffin, sliced in 4–5 μm thickness and stained with haematoxylin–eosin dye for photomicroscopy (B1 series, Motic, China). Individual liver tissue in all other cases were crushed in a tissue homogenizer and 10%*w*/*v* tissue homogenates were prepared with cold 50 mM sodium phosphate buffer (pH 7.0) containing 0.1 mM EDTA. Solutions were centrifuged at 6000×g at 4°C for 10 min and the supernatant was used for estimation of GSH (17).

Extent of lipid peroxidation was estimated spectrophotometrically, in the tissue homogenates, following estimation of MDA (malondialdehyde) in thiobarbituric acid reaction (18). Superoxide dismutase (SOD; EC1.15.1.1) in the liver was assayed at 480 nm based on the inhibitory effect on epinephrine autooxidation to adrenochrome in an alkaline medium (pH 10.2) (19) and the catalase (CAT; EC 1.11.1.6) activity were measured at 240 nm from the rate of decomposition reactions of H_2O_2 (20).

Nanoparticles Localization in Liver

Nanoparticles with or without heparin functionalization were studied for hepatic localization in both normal and APAP toxic conditions. All male Swiss albino mice (25–30 g) were divided into normal (A) and APAP treated (B) groups of 12 animals each. Group B animals were injected with 300 mg/Kg APAP i.p. and group A served as normal. Animals in group A and group B were subdivided equally and treated intravenously either with fluorescently labeled nanoparticles Fnp (subgroup I) or Hep-Fnp I (subgroup II) or Hep-Fnp II (subgroup III). One hour after this treatment, half of the animals were sacrificed by cervical dislocation under ether anesthesia and the individual liver tissue portions were dissected out. Rest were sacrificed after 3 h of treatment. The liver tissue in each case was fixed in 10%*v*/*v* formalin solution and embedded in a paraffin block, microtomed to a thickness of approximately 5 μm and were observed under confocal microscope (BD Pathway, USA). The images captured were further studied in terms of pixel intensity using ImageJ Software and the corrected total fluorescence emanating (CTCF) (21) was quantified for comparative analysis.

$$\text{CTCF} = \text{Integrated Density} - (\text{Area of Selection} \times \text{Mean fluorescence of Background})$$

Statistical Analysis

Experimental results were expressed as mean ± standard deviation. Statistical difference of mean values was evaluated following student's *t*-test. *P* values less than 0.01 were considered statistically significant.

RESULTS

AG Nanoparticles and Characterization

New nanoparticles were developed in order to fully explore the therapeutic potential of AG. Solubility characteristics of PLGA biopolymer and that of AG were quite similar and this advantage was used to adopt a simple emulsion and solvent evaporation technique for nanoparticulation. Several trial and run experiments were initially carried out to arrive at a suitable particle parameter and higher loading efficiency. Particle parameters for final nanoparticle types are presented in Table I. Heparin functionalization of nanoparticles was considered interesting for a number of advantages including anticoagulation and inhibition of angiogenesis (22). Unlike earlier attempts of chemical functionalization with heparin on nanoparticles (22) we proposed, a facile one pot nanoparticle formulation following a molecular association on PLGA. Null or two different concentrations of heparin were used and dissolved alongside stabilizer pluoronic F-127 in water media. Negative zeta potential was recorded in case of AGnp and heparin bedecked nanoparticles Hep-AGnp I and II showed further negative ζ shift due to exposed heparin carboxylates. Similar observations were also recorded in case of Hep-Fnp I and Hep-Fnp II when FITC was used as the loadable in place of AG. Particle polydispersity values were marginally higher when higher percentage of heparin was used in the preparative stages. This could be reasoned due to larger ζ charge and particle architecture. Nanoparticle entrapment efficiency was 83.42% in AGnp and was consistent in heparin functionalized nanoparticles Hep-AGnp I and II, indicating not much loss of loadable compound in preparative stages.

AFM visualization of all nanoparticle types appeared smooth and Hep-AGnp II particles were of larger z height as compared to AGnp or Hep-AGnp I (Fig. 1). Fluorescently labeled nanoparticles Hep-Fnp I and Hep-Fnp II were also examined under AFM for structural integrity. Particles were smooth on the surface and not much different than AG carrying nanoparticles

Heparin Functionalization

Heparin is a typical polyelectrolyte glycosaminoglycan, having high negative charge in aqueous environment. Immobilized heparin mass on nanoparticles were analyzed from the heparin mass originally incorporated and the free heparin molecules left in the supernatant after preparation. A tautomeric imino base, toluidine blue, reacts with heparin

Table I Nanoparticle Characteristics and Entrapment Efficiency

Nanoparticle types	Particle size nm	Polydispersity index	AG entrapment efficiency %	Zeta potential mV
AGnp	181 ± 12.60	0.115 ± 0.01	83.42 ± 3.50	−29.7 ± 1.41
Hep-AGnp I	203 ± 16.32$^{\$}$	0.162 ± 0.01*	82.91 ± 3.70	−41.5 ± 2.03*
Hep-AGnp II	216 ± 18.21*	0.213 ± 0.01*	82.07 ± 3.64	−43.41 ± 2.08*
Hep-Fnp I	198 ± 11.03$^{\$}$	0.147 ± 0.01*	–	−37.98 ± 1.67*
Hep-Fnp II	209 ± 19.66$^{\$}$	0.205 ± 0.02*	–	−41. 27 ± 1.78*
Fnp	174 ± 11.61$^{\Upsilon}$	0.143 ± 0.01*	–	−25.44 ± 2.47$^{\$}$

Results expressed as mean ± Standard Deviation ($n = 4$); *$p < 0.01$; significant difference compared with AGnp. $^{\$}$ $P < 0.1$; $^{\Upsilon}$ $P < 0.5$; no significant difference compared with AGnp.

molecules, resulting in a concentration dependent absorbance peak shift from 630 nm to 562 nm (15). This reaction was used to estimate the amount of heparin entrapped on different nanoparticles prepared. A standard graph, y = 0.0384x + 0.1278, $R^2 = 0.9928$, was first developed from the recorded absorbance (y) for a known heparin concentration (x) reacting with a fixed amount of toluidine blue (10 µg/ml). In case of Hep-AGnp I nanoparticles 76.13 ± 2.66% of heparin was observed entrapped while in Hep-AGnp II, 71.79 ± 3.71% of heparin was entrapped. This indicated a near saturated condition of heparin when 1 mg/ml of heparin was initially used. Similar observations were recorded in case of FITC labeled nanoparticles Hep-Fnp I and Hep-Fnp II where heparin entrapments were recorded to be 65.28 ± 2.51% and 66.36 ± 2.09% respectively.

FT IR studies

FT IR spectra of polymer components and AG are presented in Fig. 2a. FT IR spectra for PLGA 50:50 was typical and the C=O stretching vibrations were recorded at 1752 cm^{-1} while the chain CH_2 stretching was recorded at 2851 cm^{-1} The bands at 1452 $cm^{-1}$and 1139 cm^{-1} were due to C–O and C–H bonds of PLGA (23). FT IR of AG in KBr presented alcoholic O–H stretching at 3402 cm^{-1} and the characteristic lactone vibrations were at 1727 cm^{-1}. The C–O stretching appeared at 1030 cm^{-1} and at 1078 cm^{-1} for the primary and secondary alcoholic functions and the CH_2 stretching in AG was recorded at 2932 cm^{-1}(14). Pluronic F127 is a Polyethylene oxide-polypropylene oxide triblock polymer and distinctive C–H stretching was observed at 2884 cm^{-1} and the archetypical C–O–C stretching vibration was recorded at 1111 cm^{-1} (24).

However in AGnp (Fig. 2b), PLGA O–H stretching vibrations at 3520 cm^{-1} was broadened with a peak shift at 3442 cm^{-1} due to polymer interactions with pluronic F-127. PLGA C=O stretching at 1752 cm^{-1} however was intact and Pluronic C–O–C stretching was shifted to 1144 cm^{-1} with reduced intensity indicating hydrogen bond interactions. Similar observations were reported earlier in case of Pluronic functionalized nanoparticles (25). Heparin interactions were predominant in both Hep-AGnp I and II nanoparticles. Typical heparin COO^- asymmetric vibrations at 1620 cm^{-1} experienced a shift at 1646 cm^{-1} in both formulations due to stabilization and hydrogen bonding. In

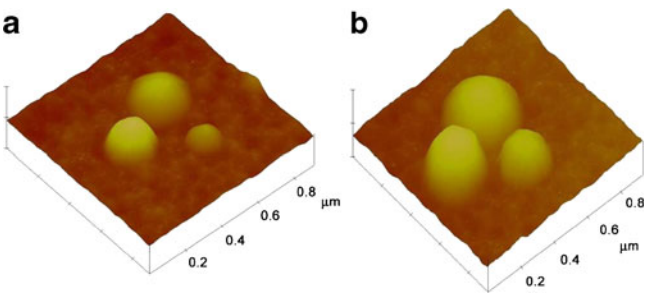

Fig. 1 Atomic force microscopy in tapping mode; (**a**) nanoparticle, AGnp; (**b**) heparin functionalized nanoparticle Hep-AGnp II.

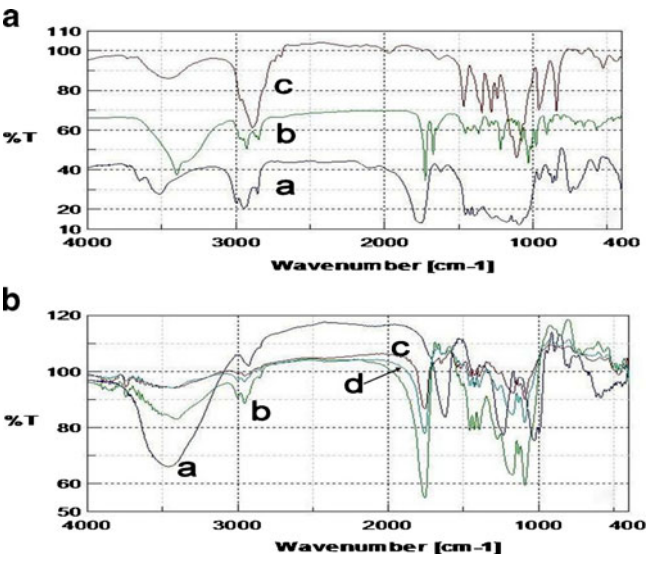

Fig. 2 FT IR Studies for polymers and nanoparticles. (**a**) FT IR spectra of *a*) PLGA (*blue*), *b*) AG (*green*) and *c*) Pluronic (*brown*); (**b**) FTIR spectra of *a*) Heparin (*blue*), *b*) Hep-AGnp I (*green*), *c*) Hep-AGnp II (*red*) and *d*) AGnp (*sky blue*).

addition PLGA –C–H stretching vibrations at 2945 cm^{-1} observed a red shift at 2997 cm^{-1} likely due to a tri molecular composite conjugation. These observations also corroborated well with PCS and zeta potential studies where a large negative shift in zeta charge was observed due to heparin functionalization.

AG Release and Kinetic Modeling

Cumulative percentage release of AG over time was recorded up to 360 h in dialysis method and the results are presented in Fig. 3. The plotted AG release response from all nanoparticle types revealed a biphasic nature with an initial rapid release phase followed by a slower and continuous release period. An initial faster *in vitro* release was noted in case of AGnp which culminated at 12 h. This phase was almost similar in case of heparin functionalized nanoparticles and about 40% of AG mass loading was released over that period. The release was much slower hence forth and 85% of the loading was traceable during the study period.

The payload release mechanism from nanoparticle cargo devices was evaluated by fitting into Korsemeyer-Peppas model. The calculated release exponent 'n' value for all three formulations (Table II) implicates that the release mechanism is not purely diffusion controlled (26). PLGA-based spherical delivery devices undergo surface erosion (27) and this might have contributed to the release phenomenon in case of AG nanoparticles.

Stability Studies

AGnp and Hep-AGnp nanoparticles were fairly stable when stored in refrigerated conditions and stability responses are presented in Fig. 4. One reason for no particle aggregation during 3 months study period could be due to typical stabilization in presence of pluronic F 127 (Fig. 4a). Pluronic molecules are known to localize on PLGA due to hydrophobic interactions of PPO blocks. The surface exposed PEO blocks of Pluronic also interacted with the

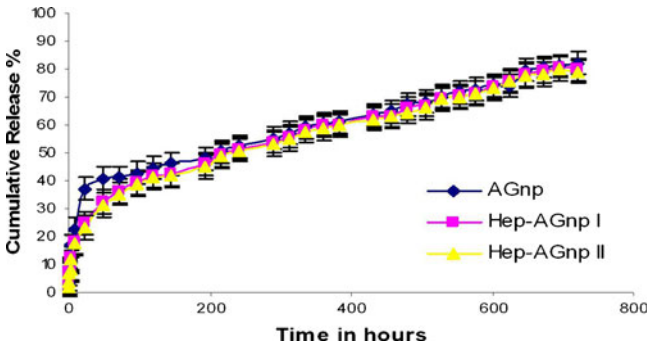

Fig. 3 Dissolution study of AG nanoparticles.

Table II AG Release Parameters in Korsemeyer-Peppas Model

Nanoparticle type	n	K
AGnp	0.34	0.11
HepAGnp I	0.39	0.08
HepAGnp II	0.41	0.07

n denotes release exponent; K denotes constant depending on structure and geometry of the device

polyelectrolyte heparin to effect stabilization. Similar reactions were earlier observed due to linking reactions between pluronic PEO groups and carboxylates in alginate (28). A minor mass leaching of 1% of AG load was however observed in the nanoparticles. This apparently might have contributed to a slight positive shift in particle zeta potential values from −41.53 mv to −39.96 mv in case of Hep-AGnp I after 3 months storage period.

Nanoparticles and APAP Hepatotoxicity

Liver enzymes escapade in the serum are reliable indicators for hepatotoxic conditions (29). Profound hepatocellular damage and intense rise in serum marker enzymes were recorded after 12 h of APAP injection (Table III). Alanine aminotransferase (ALT) activity increased many folds in serum alongside aspartate aminotransferase (AST) and alkaline phosphatase (ALP) in APAP treated group as compared to control ($p<0.001$). Treatment with AG in group 3 decreased the activities of marker enzymes in comparison with the APAP treated group ($p<0.001$). Escape of liver enzymes in the serum however was significantly reduced ($p<0.001$) in group 5 and 6 when animals were treated with Hep-AGnp I or Hep-AGnp II. Effects of Hep-AGnp I and II were significantly more pronounced when compared to AG ($p<0.001$) or AGnp ($p<0.001$). Reduced glutathione level (GSH) in liver tissue was also monitored as it could be directly linked to APAP hepatotoxicity. The level of GSH was lowered at 6.8 ± 0.83 μ mole/gm in group 2 animals treated with APAP. Depletion of glutathione level was restored significantly in the treatment groups as compared to the group receiving APAP alone. GSH levels were near normal levels in group 5 and

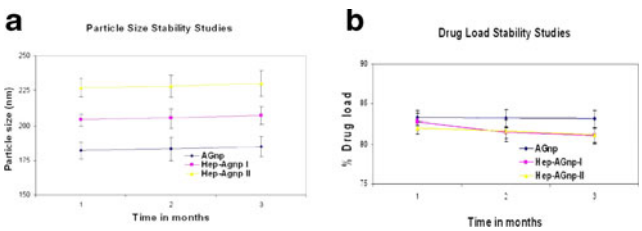

Fig. 4 Nanoparticles stability studies: (**a**) particle size, (**b**) drug load.

Table III AG Nanoparticle Treatment in APAP Induced Liver Damage

Test groups	Aspartate serum transmainse (IU/L)	Alanine transmainase (IU/L)	Alakaline phosphatase (IU/L)	Reduced glutathione (μ mole/gm of tissue)
Group 1	80.33 ± 14.71*	97.21 ± 16.83*	127.21 ± 19.33*	16.20 ± 1.54*
Group 2	3519 ± 311.61	4007 ± 383.50	1659 ± 130.72	6.83 ± 0.83
Group 3	1268 ± 182.94*	1359 ± 177.45*	927 ± 88.19*	9.32 ± 0.87*
Group 4	576 ± 69.03*	631 ± 77.22*	308.73 ± 27.94*	11.92 ± 0.93*
Group 5	372 ± 32.53*	406 ± 55.68*	204.5 ± 25.72*	14.85 ± 0.51*
Group 6	386 ± 42.29*	418 ± 50.27*	209.8 ± 20.33*	14.37 ± 0.57*

Results expressed as mean ± Standard Deviation ($n = 8$), *$p < 0.001$; significant difference compared to APAP treated group. IU/L denotes International Units per Litre.

group 6. Regeneration of GSH in nanoparticle treated groups can possibly be linked to an appropriate regeneration due to AG localization. These results show concurrence with the liver histology observations where maximum restoration was achieved in Hep-AGnp I and II treated groups.

Liver Histopathology

Histopathology analyses of mouse liver from different treated groups are presented in Fig. 5. Mouse liver section from APAP treated group revealed severe centrilobular necrosis with inflammatory cell infiltration and sinusoidal dilatation (Fig. 5b). Normal control animals exhibited regular hepatic architecture, prominent central vein, sinusoidal spaces, well preserved cytoplasm and prominent nucleus (Fig. 5a). In AGnp treated group improvement in liver architecture was observed associated with a moderate inflammatory cell infiltration. Significant recovery was noted in Hep-AGnp I and Hep-AGnp II treated group 5 and 6. Hepatic necrosis was attenuated and well formed liver cytoarchitecture were recorded in these cases. These results indicated a considerable normalization effect due to engineered nanoparticle types Hep AGnp I and II.

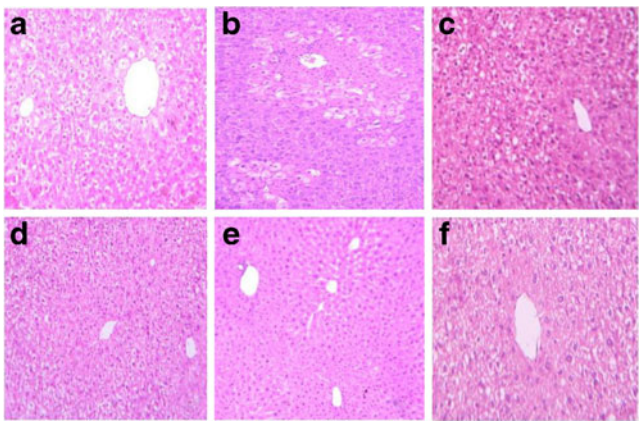

Fig. 5 Liver Histopathology Study acquired at 40x. (**a**) Group 1, normal; (**b**) Group 2, APAP; (**c**) Group 3, APAP and AG; (**d**) Group 4, APAP and AGnp; (**e**) Group 5, APAP and Hep-AGnp II; (**f**) Group 6, APAP and Hep-AGnp I.

Effects on Lipid Peroxidation and Hepatic Antioxidant Enzymes

Reactive oxygen species (ROS) and oxidative stress are linked to APAP induced hepatic necrosis (30). Elevated MDA levels are a convenient index for lipid peroxidation related oxidative damage in APAP intoxication. ROS generated in hepatocytes due to APAP overdose can be detoxified by specific enzymes such as superoxide dismutase which converts superoxide anion (O_2^{0-}) into hydrogen peroxide (H_2O_2), which in turn is detoxified by catalase, glutathione peroxidase and thioredoxin (31). MDA activity was enhanced by 63% ($p < 0.001$) in group 2 animals as compared to group 1 and hepatic antioxidant enzymes SOD and CAT were decreased indicating a typical oxidative stress induced by APAP. Though AG reduced MDA activity it however induced little effect in activity of SOD and CAT. In comparison, the composite nanoparticles Hep-AGnp I and II persuaded a near normal effect in SOD ($p < 0.001$) and CAT ($p < 0.001$) activity (Fig. 6). This was considered plausible due to AG biochemical pharmacology and rapid migration of nanoparticles up to the liver tissue.

Localization in Liver Experiments

Encouraged by the APAP hepatotoxicity results, nanoparticles localization in the liver tissue was separately evaluated. Nanoparticles traverse through multiple pathways of systemic circulation and localization of fluorescently labeled nanoparticles in the liver was recorded at hourly intervals after an intravenous injection. FITC labeled nanoparticles were localized in the liver within 1 h of intravenous injection. Fluorescent nanoparticle localization was maximal after 3 h of injection (Fig. 7). Confocal microscopy image for Hep-Fnp I and II treated groups were very intense as compared to Fnp treated liver (Fig. 7). It was interesting to note that fluorescent intensity in Hep-Fnp I and II treated

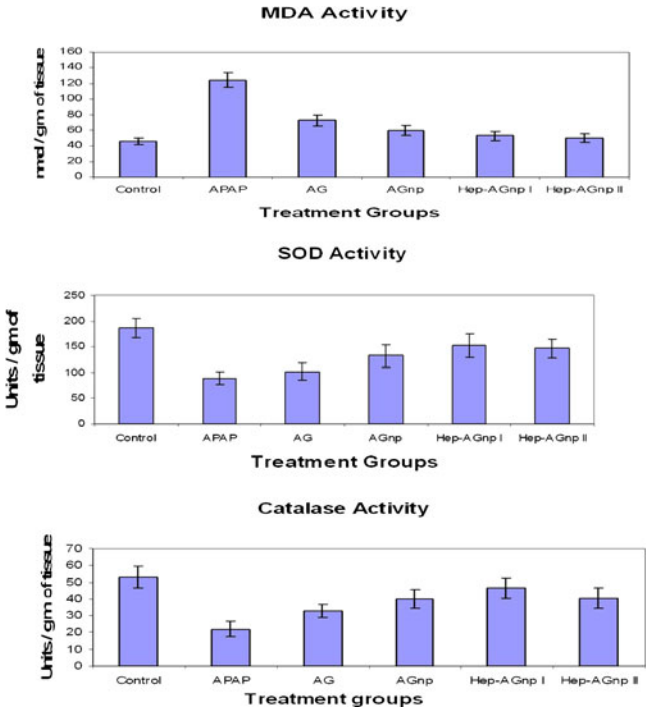

Fig. 6 Effect of APAP, AG and nanoparticles on Malonedialdehyde, Superoxide Dismutase and Catalase activity in mouse liver.

groups were greater in APAP treated liver compared to normal liver sections. Fluorescent pixel intensity was further evaluated from 10 number of liver section images captured in each study group and the corrected total fluorescence was plotted as an indicator of nanoparticle liver tissue localization for comparison (Fig. 8). It was very clear from the intensity analysis study that heparin bedecked composite nanoparticles were localized within 1 h in the liver tissue.

DISCUSSION

APAP overdose is most prevalent among the drug induced liver injuries. Unlike other DILD, hepatotoxicity due to APAP is more clearly understood (32). Despite favorable prognosis, the management of poisoning however is a challenge for health care professionals, pharmaceutical industry and regulatory authorities. AG is known to exert multiple effects on liver tissue. *Andrographis paniculata* extract was earlier demonstrated as one of the most potent hepatoprotectants (33,34). AG, the diterpene lactone strongly induces mRNA synthesis and protein expression in hepatocytes primary culture (35). Like *Panax ginseng*, *Andrographis* extracts have a marked effect on hepatic phase I biotransformation enzymes (CYP 1A and 2B) (36). AG also differentially activates GST isozymes indicating a role in chemical detoxification. Synthesis of prodrugs and formulation solubility enhancements were earlier attempted

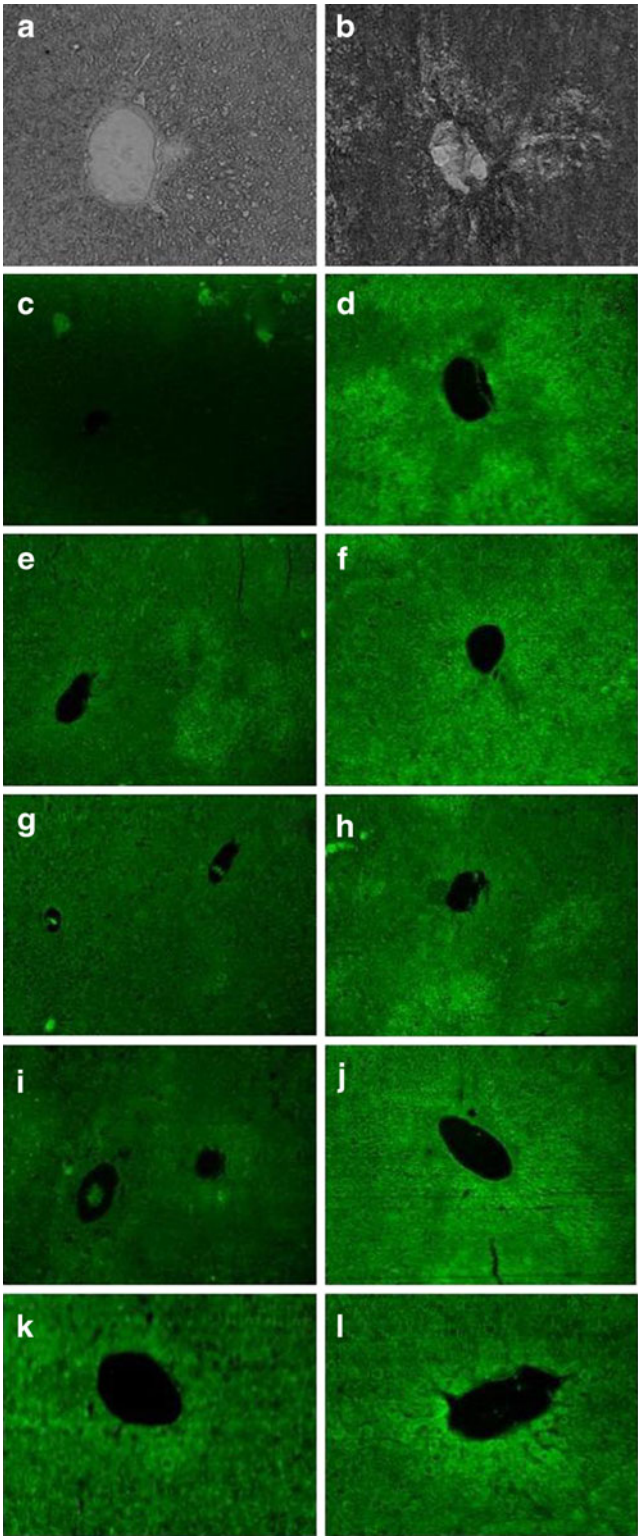

Fig. 7 Nanoparticle localization in liver. Transmitted optical microscopy image of (**a**) normal liver and (**b**) APAP damaged liver. Fluorescent microscopy image; Fnp-treated (**c**) normal liver and (**d**) APAP damaged liver after 1 h. Hep-Fnp I-treated (**e**) normal liver and (**f**) APAP damaged liver, after 1 h. Fnp-treated (**g**) normal liver and (**h**) APAP damaged liver, after 3 h. Hep-Fnp II-treated (**i**) normal liver and (**j**) APAP damaged liver, after 3 h. Hep-Fnp I-treated (**k**) normal liver and (**l**) APAP damaged liver, after 3 h.

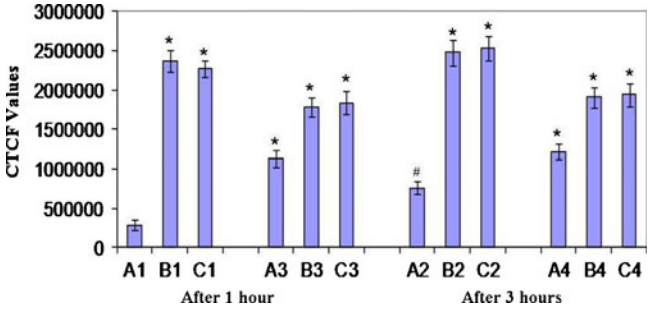

Fig. 8 Pixel quantitative analysis of nanoparticle localization in liver. Normal liver after 1 h,A1,B1,C1; APAP damaged liver after 1 h A3,B3,C3; Normal liver after 3 h, A2,B2,C2; APAP damaged liver after 3 h, A4,B4,C4. A=Fnp; B=Hep-Fnp I and C=Hep-Fnp II. Results expressed as mean ± SE ($n=4$); *$p<0.01$ significant difference compared with A1. #$p<0.1$, no significant difference compared with A1.

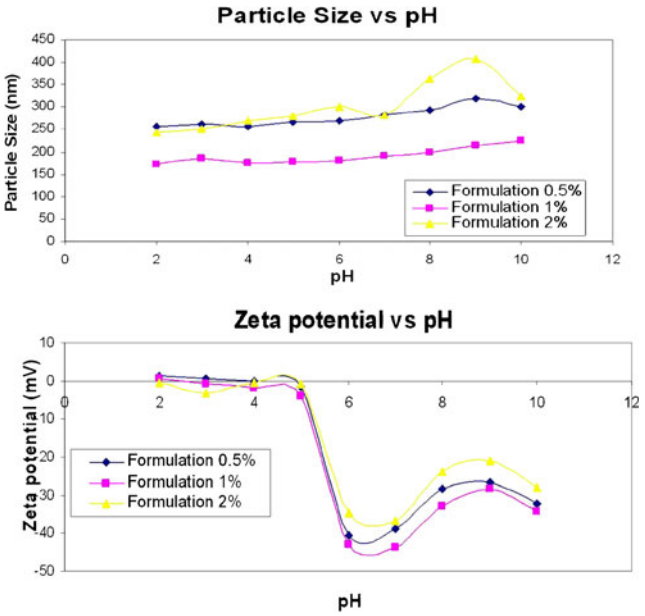

Fig. 9 Changes in particle size and zeta potential of AG nanoparticles (AGnp) in pH range 2–10.

to exploit therapeutic potentials of AG. The KCE therefore is a potent chemopreventive requiring delivery development.

In the present study, we prepared nanoparticles for exploiting hepatoprotective activity against experimental APAP overdose. Pluronic F-127 (or Poloxamer 407) is a US FDA approved non ionic surfactant that stabilizes PLGA nanospheres actively in systemic circulation (37). Unlike PVA which forms hydrophilic sheath layer over nanoparticles, pluronics interact in both hydrophobic and hydrophilic domain. The polyoxyethylene-polyoxypropylene triblock copolymer PF-127, adsorb on water deficient surfaces rigidly with polyoxypropylene groups while polyoxyethylene groups are exposed in water interface. Pluronics assume concentration dependent structural orientations and different particle stabilization studies are interesting in water environment (38).

Effect of pluoronic concentration on nanoparticle hydrodynamic diameter and electrophoretic mobility over a pH range was studied initially to attain a typical stabilization for AG nanoparticles. Nanoparticles were prepared varying stabilizer PF-127 concentration (0.5, 1 and 2%*w/v*) and were observed over a pH range of 2 to 10. Particle size was consistent and lower when 1%*w/v* pluronic was used in the reaction mixture (Fig. 9). At higher concentration of 2%*w/v* a degree of particle aggregation was observed in PCS correlograph around pH 7. At lower concentration of 0.5%, a higher average particle size was observed. This was possibly due to PEO chain conformation and particle surface not being fully covered with the stabilizer (38). Zeta potential values were consistently lower at around pH 7 indicating stability near that region. Higher pluronic concentration possibly helped collate at higher pH ranges as indicated in size and zeta analysis.

AG loading was consistent in all nanoparticles types but a variation was noted in zeta potential values (Table I). This was likely due to a formation of composite nanoparticles structure from non covalent polymer interactions. Heparin COO^- groups further lowered the particle zeta potential values in case of Hep-AGnp I and II. Cumulative AG release pattern was almost similar in all cases but the mass and rate release was lower in case Hep-AGnp I in initial hours. Composite polymer nanostructure was one another reason that imparted excellent particle stability over the period of study as observed in stability studies (Fig. 4).

Heparin immobilization in pluronic stabilized nanoparticles is likely due to composite polymer interactions (39,40). Nanoparticle polymer interactions were clearly observed in detailed FT-IR studies (Fig. 2). The polymer O–H stretching vibrations near 3520 cm^{-1} were significantly reduced in intensity due to hydrogen bond interactions. Heparin mass immobilization observations in UV experiments were also confirmatory for molecular immobilization due to composite interactions. Sequential steps for synthesis of new engineered AG loaded nanoparticles are depicted schematically in Fig. 10.

New engineered nanoparticles could rapidly localize up to the liver as observed in fluorescence studies. Composite nanoparticles Hep-Fnp I and II were effectively localized both in normal and APAP hepatoxic conditions. Fluorescent pixel intensity in APAP damaged liver was more in 1 h due to engineered nanoparticle tracing up to the hepatocellular sites. Functionalized nanoparticle localization in liver was rapid and higher fluorescence was recorded after 3 h of intravenous injection in case of Hep-Fnp I and II (Fig. 8).

APAP hepatotoxicity is reportedly caused by the formation of NAPQ I and marked by abrupt increase of serum AST, ALT, and ALP levels. Similar observations were recorded in biochemical studies but were abrogated when treated with nanoparticles Hep-AGnp I and II. Engineered AG nanoparticles therefore are in favorable disposition to mitigate APAP overdose hepatotoxicity. The centrilobular hepatic necrosis

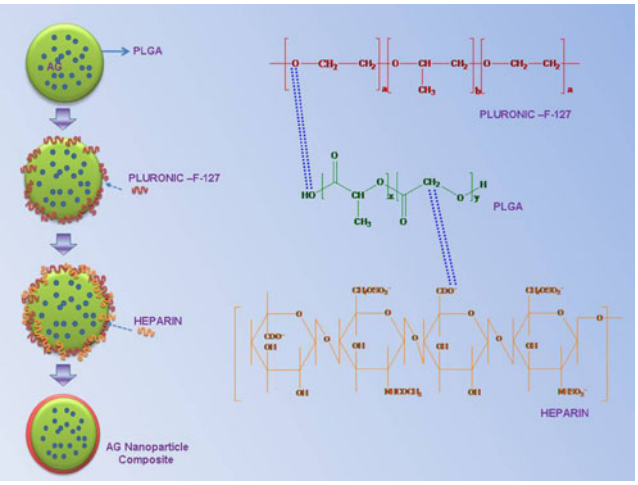

Fig. 10 Sequential steps in formation of Composite AG nanoparticles.

associated with ballooning degeneration typical in APAP histopathology was remarkably reverted in treatment with new AG nanoparticles. This was further indicative of rapid hepatic localization of composite nanostructures that helped regeneration of hepatocytes.

GSH is an important sulfhydryl that maintains cellular macromolecules in functional state and serves as a key determinant of the extent of APAP induced hepatic injury (41). Prolonged treatment with AG extracts has been shown earlier to increase the cellular nonprotein thiol levels *in vivo* (42). Our data clearly showed an up-regulation GSH in liver by AGnps' and more particularly the Hep-AGnp I and II. The results demonstrated that, increased cellular GSH level is one responsible factor for the hepatoprotective action of AG and nanoparticles. The redox-dependent regulation of GSH synthesis is controlled by the induction of cellular proteins. APAP induced excess levels of ROS which lead to enhancement of lipid peroxidation and reduction of antioxidant enzyme activity. This is responsible for further attack on biological molecules like proteins, phospholipids and DNA (43). AG nanoparticles Hep AGnp I and II have effectively enhanced SOD and CAT antioxidant enzyme activity and diminished lipid peroxidation indicator levels. Our results established that the composite type nanoparticles with AG load are useful agents against specific drug induced hepatotoxicity. Further the biomolecular effects of the pleotropic agent AG can be preserved in engineered nanoparticles for an enhanced efficacy.

AG reportedly is more effective than Silymarin in hepatic injury (33). Unlike Silymarin soluble derivative that is currently being evaluated in intravenous therapy against severe hepatic injury (44), the new composite nanoparticles for AG extended hepatoprotection following particle directed transport. Having achieved liver directed AG nanoparticles we are currently focused to explore the pharmacokinetics through oral routes.

CONCLUSIONS

In this study we report a facile one pot synthesis for composite heparin functionalized PLGA nanoparticles. Nanoparticles loaded with a KCE, AG were evaluated for the first time as an efficient therapeutic against APAP induced progressive hepatotoxicity. Furthermore, functionalized nanoparticles could localize rapidly in the liver and up regulate hepatic GSH store. Hepatic localization of nanoparticles also favorably promotes anti oxidant capacity in the liver. Thus, new AG nanoparticles can be useful in several areas including as a protective agent against liver damage in APAP overdose.

ACKNOWLEDGMENTS AND DISCLOSURES

Senior Research Fellowships to Partha Roy and Suvadra Das from Indian Council for Medical Research and Council of Scientific and Industrial Research respectively, is gratefully acknowledged. This work is partly funded from the Department of Biotechnology Govt of India nanoscience and nanotechnology grants. Dr. Runa Ghosh Auddy would like to thank CRNN, University of Calcutta for financial assistance.

REFERENCES

1. Lee WM. Acetaminophen-related acute liver failure in the United States. Hepatol Res. 2008;38(Suppl1):S3–8.
2. Knight TR, Fariss MW, Farhood A, Jaeschke H. Role of lipid peroxidation as a mechanism of liver injury after acetaminophen overdose in mice. Toxicol Sci. 2003;76(1):229–36.
3. Chen C, Hennig GE, Manautou JE. Hepatobiliary excretion of acetaminophen glutathione conjugate and its derivatives in transport-deficient (TR-) hyperbilirubinemic rats. Drug Metab Dispos. 2003;31(6):798–804.
4. Knight TR, Kurtz A, Bajt ML, Hinson JA, Jaeschke H. Vascular and hepatocellular peroxynitrite formation during acetaminophen toxicity: role of mitochondrial oxidant stress. Toxicol Sci. 2001;62(2):212–20.
5. Jaeschke H, McGill MR, Williams CD, Ramachandran A. Current issues with acetaminophen hepatotoxicity—a clinically relevant model to test the efficacy of natural products. Life Sci. 2011;88(17–18):737–45.
6. North TE, Babu IR, Vedder LM, Lord AM, Wishnok JS, Tannenbaum SR, *et al.* PGE2-regulated wnt signaling and N-acetylcysteine are synergistically hepatoprotective in zebrafish acetaminophen injury. Proc Natl Acad Sci U S A. 2010;107(40):17315–20.
7. Hidalgo MA, Romero A, Figueroa J, Cortes P, Concha II, Hancke JL, *et al.* Andrographolide interferes with binding of nuclear factor-kappaB to DNA in HL-60-derived neutrophilic cells. Br J Pharmacol. 2005;144(5):680–6.
8. Trivedi NP, Rawal UM, Patel BP. Hepatoprotective effect of andrographolide against hexachlorocyclohexane-induced oxidative injury. Integr Cancer Ther. 2007;6(3):271–80.

9. Sheeja K, Guruvayoorappan C, Kuttan G. Antiangiogenic activity of Andrographis paniculata extract and andrographolide. Int Immunopharmacol. 2007;7(2):211–21.
10. Zhu SP, Kang BA. Distribution and excretion of [35S] NaHSO3-andrographolide by autoradiography. Acta Pharmacol Sin. 1981;2 (4):266–9.
11. Yuasa H, Watanabe J. Are novel scavenger-like receptors involved in the hepatic uptake of heparin? Drug Metab Pharmacokinet. 2003;18(5):273–86.
12. Sun IC, Eun DK, Na JH, Lee S, Kim IJ, Youn IC, *et al.* Heparin-coated gold nanoparticles for liver-specific CT imaging. Chemistry. 2009;15(48):13341–7.
13. Park K, Kim K, Kwon IC, Kim SK, Lee S, Lee DY, *et al.* Preparation and characterization of self-assembled nanoparticles of heparin-deoxycholic acid conjugates. Langmuir. 2004;20 (26):11726–31.
14. Roy P, Das S, Bera T, Mondol S, Mukherjee A. Andrographolide nanoparticles in leishmaniasis: characterization and *in vitro* evaluations. Int J Nanomed. 2010;5:1113–21.
15. Wirsen A, Ohrlander M, Albertsson AC. Bioactive heparin surfaces from derivatization of polyacrylamide-grafted LLDPE. Biomaterials. 1996;17(19):1881–9.
16. Mladenovic D, Radosavljevic T, Ninkovic M, Vucevic D, Jesic-Vukicevic R, Todorovic V. Liver antioxidant capacity in the early phase of acute paracetamol-induced liver injury in mice. Food Chem Toxicol. 2009;47(4):866–70.
17. Ellman GL. Tissue sulfhydryl groups. Arch Biochem Biophys. 1959;82(1):70–7.
18. Ohkawa H, Ohishi N, Yagi K. Assay for lipid peroxides in animal tissues by thiobarbituric acid reaction. Anal Biochem. 1979;95 (2):351–8.
19. Misra HP, Fridovich I. The generation of superoxide radical during the autoxidation of hemoglobin. J Biol Chem. 1972;247 (21):6960–2.
20. Best TM, Fiebig R, Corr DT, Brickson S, Ji L. Free radical activity, antioxidant enzyme, and glutathione changes with muscle stretch injury in rabbits. J Appl Physiol. 1999;87(1):74–82.
21. Gavet O, Pines J. Progressive activation of CyclinB1-Cdk1 coordinates entry to mitosis. Dev Cell. 2010;18(4):533–43.
22. Kemp MM, Kumar A, Mousa S, Dyskin E, Yalcin M, Ajayan P, *et al.* Gold and silver nanoparticles conjugated with heparin derivative possess anti-angiogenesis properties. Nanotechnology. 2009;20(45):1–7.
23. Meng ZX, Zheng W, Li L, Zheng YF. Fabrication, characterization and *in vitro* drug release behavior of electrospun PLGA/chitosan nanofibrous scaffold. Mater Chem Phys. 2011;125(3):606–11.
24. Innocenzi P, Malfatti L, Piccinini M, Marcelli A. Evaporation-induced crystallization of pluronic F127 studied *in situ* by time-resolved infrared spectroscopy. J Phys Chem A. 2010;114(1):304–8.
25. Yuk SH, Oh KS, Cho SH, Kim SY, Oh S, Lee JH, *et al.* Enhancement of the targeting capabilities of the Paclitaxel-loaded pluronic nanoparticles with a glycol chitosan/heparin composite. Mol Pharm. 2012;9(2):230–6.
26. Grattard N, Pernin M, Marty B, Roudaut G, Champion D, Le Meste M. Study of release kinetics of small and high molecular weight substances dispersed into spray-dried ethylcellulose microspheres. J Control Release. 2002;84(3):125–35.
27. Siepmann J, Siepmann F. Mathematical modeling of drug delivery. Int J Pharm. 2008;364(2):328–43.
28. Lin HR, Sung KC, Vong WJ. *In situ* gelling of alginate/pluronic solutions for opthalmic delivery of pilocarpine. Biomacromolecules. 2004;5(6):2358–65.
29. Marschall HU, Wagner M, Zollner G, Trauner M. Clinical hepatotoxicity regulation and treatment with inducers of transport and cofactors. Mol Pharm. 2007;4(6):895–910.
30. Hinson JA, Roberts DW, James LP. Mechanisms of acetaminophen-induced liver necrosis. In: Uetrecht J, editor. Adverse drug reactions, handbook of experimental pharmacology. Berlin Heidelberg: Springer-Verlag; 2010. p. 369–405.
31. Ferret PJ, Hammoud R, Tulliez M, Tran A, Trebeden H, Jaffray P, *et al.* Detoxification of reactive oxygen species by a nonpeptidyl mimic of superoxide dismutase cures acetaminophen-induced acute liver failure in the mouse. Hepatology. 2001;33(5):1173–80.
32. Jaeschke H, Bajt ML. Intracellular signaling mechanisms of acetaminophen-induced liver cell death. Toxicol Sci. 2006;89 (1):31–41.
33. Visen PKS, Shukla B, Patnaik GK, Dhawan BN. Andrographolide protects rat hepatocytes against paracetamol-induced damage. J Ethnopharmacol. 1993;40(2):131–6.
34. Shi G, Zhang Z, Zhang R, Zhang X, Lu Y, Yang J, *et al.* Protective effect of andrographolide against concanavalin A-induced liver injury. Naunyn Schmiedebergs Arch Pharmacol. 2012;385(1):69–79.
35. Chang KT, Lii CK, Tsai CW, Yang AJ, Chen HW. Modulation of the expression of the pi class of glutathione S-transferase by Andrographis paniculata extracts and andrographolide. Food Chem Toxicol. 2008;46(3):1079–88.
36. Jarukamjorn K, Don-in K, Makejaruskul C, Laha T, Daodee S, Pearaksa P, *et al.* Impact of Andrographis paniculata crude extract on mouse hepatic cytochrome P450 enzymes. J Ethnopharmacol. 2006;105(3):464–7.
37. Dunn SE, Coombes AGA, Garnett MC, Davis SS, Davies MC, Illum L. *In vitro* cell interaction and *in vivo* biodistribution of poly(lactide-co-glycolide) nanospheres surface modified by poloxamer and poloxamine copolymers. J Control Release. 1997;44(1):65–76.
38. Santander-Ortega MJ, Jodar-Reyes AB, Csaba N, Bastos-Gonzalez D, Ortega-Vinuesa JL. Colloidal stability of pluronic F68-coated PLGA nanoparticles: a variety of stabilisation mechanisms. J Colloid Interface Sci. 2006;302(2):522–9.
39. Oh KS, Song JY, Yoon SJ, Park Y, Kim D, Yuk SH. Temperature-induced gel formation of core/shell nanoparticles for the regeneration of ischemic heart. J Control Release. 2010;146(2):207–11.
40. Besheer A, Vogel J, Glanz D, Kressler J, Groth T, Mäder K. Characterization of PLGA nanospheres stabilized with amphiphilic polymers: hydrophobically modified hydroxyethyl starch *vs* pluronics. Mol Pharm. 2009;6(2):407–15.
41. Fakurazi S, Hairuszah I, Nanthini U. Moringa oleifera Lam prevents acetaminophen induced liver injury through restoration of glutathione level. Food Chem Toxicol. 2008;46 (8):2611–5.
42. Trivedi NP, Rawal UM. Hepatoprotective and antioxidant property of Andrographis paniculata (Nees) in BHC induced liver damage in mice. Indian J Exp Biol. 2001;39(1):41–6.
43. Hinson JA, Reid AB, McCullough SS, James LP. Acetaminophen-induced hepatotoxicity: role of metabolic activation, reactive oxygen/nitrogen species, and mitochondrial permeability transition. Drug Metab Rev. 2004;36(3–4):805–22.
44. Mehrab-Mohseni M, Sendi H, Steuerwald N, Ghosh S, Schrum LW, Bonkovsky HL. Legalon-SIL downregulates HCV core and NS5A in human hepatocytes expressing full-length HCV. World J Gastroenterol. 2011;17(13):1694–700.